

High-performance broadband photodetector based on PdSe₂/black phosphorus heterodiode

Cite as: Appl. Phys. Lett. **120**, 231103 (2022); <https://doi.org/10.1063/5.0097044>
 Submitted: 25 April 2022 • Accepted: 26 May 2022 • Published Online: 07 June 2022

Qingsong Dong, Fang Wang, Xin Hu, et al.



View Online



Export Citation



CrossMark

ARTICLES YOU MAY BE INTERESTED IN

[40 GHz waveguide-integrated two-dimensional palladium diselenide photodetectors](#)
 Applied Physics Letters **120**, 231102 (2022); <https://doi.org/10.1063/5.0091625>

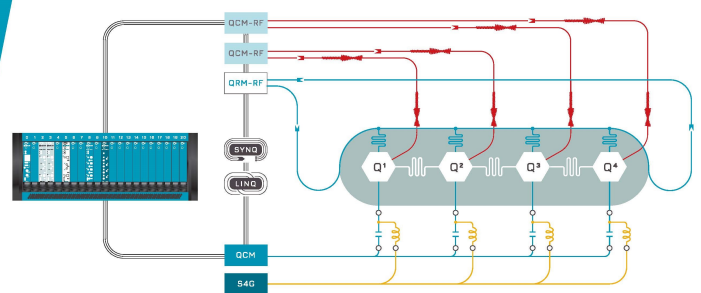
[MoS₂/SnO₂ heterojunction-based self-powered photodetector](#)
 Applied Physics Letters **120**, 181106 (2022); <https://doi.org/10.1063/5.0087652>

[Strong interfacial coupling in vertical WSe₂/WS₂ heterostructure for high performance photodetection](#)
 Applied Physics Letters **120**, 181108 (2022); <https://doi.org/10.1063/5.0082101>

 QBLOX

Integrates all
 Instrumentation + Software
 for Control and Readout of
Superconducting Qubits

[visit our website >](#)



High-performance broadband photodetector based on PdSe₂/black phosphorus heterodiode

Cite as: Appl. Phys. Lett. **120**, 231103 (2022); doi: 10.1063/5.0097044

Submitted: 25 April 2022 · Accepted: 26 May 2022 ·

Published Online: 7 June 2022



View Online



Export Citation



CrossMark

Qingsong Dong,¹ Fang Wang,² Xin Hu,¹ Yuan Lu,³ Dongxu Zhao,⁴ Min Zhang,^{5,a)}  Tao Han,¹  Xingyuan Hou,¹ Shaoliang Wang,¹ Mingsheng Long,^{1,a)}  and Lei Shan¹ 

AFFILIATIONS

¹Information Materials and Intelligent Sensing Laboratory of Anhui Province, Key Laboratory of Structure and Functional Regulation of Hybrid Materials of Ministry of Education, Institutes of Physical Science and Information Technology, Anhui University, 111 Jiu Long Road, Hefei 230601, China

²State Key Laboratory of Infrared Physics, Shanghai Institute of Technical Physics, Chinese Academy of Sciences, 500 Yu Tian Road, Shanghai 200083, China

³Infrared and Low-Temperature Plasma Key Laboratory of Anhui Province, State Key Laboratory of Pulsed Power Laser Technology, 460 Huangshan Road, NUDT, Hefei 230037, China

⁴State Key Laboratory of Luminescence and Applications, Changchun Institute of Optics, Fine Mechanics and Physics, Chinese Academy of Sciences, 3888 Dongnanhu Road, Changchun 130033, China

⁵College of Data Science, Jiaying University, No.899 Guangqiong Road, Jiaying, Zhejiang 314001, China

^{a)}Authors to whom correspondence should be addressed: zhangm16@fudan.edu.cn and longms@ahu.edu.cn

ABSTRACT

Uncooled long-wavelength infrared photodetectors based on two-dimensional materials have wide applications, such as remote sensing, missile guide, imaging, and night vision. However, realizing high-performance photodetectors based on 2D materials with high photoresponsivity and fast response speed is still a challenge. Here, we report an ultra-broadband photodetector based on the PdSe₂/BP van der Waals heterodiode with a fast response speed. The detection range of the PdSe₂/BP heterodiode is covered from visible to long-wave infrared (0.4–10.6 μm). A high photoresponsivity of 116.0 A/W and a low noise equivalence power of 8.4×10^{-16} W/Hz^{1/2} and D^* of 2.05×10^9 cm Hz^{1/2}/W were demonstrated. Notably, the heterodiode exhibits a very fast response speed with $\tau_r = 2.9$ and $\tau_d = 4.0$ μs. Our results introduced a promising application in broadband and fast photoresponse at weak light intensity.

Published under an exclusive license by AIP Publishing. <https://doi.org/10.1063/5.0097044>

Since the discovery of two-dimensional (2D) material graphene, black phosphorus (BP) and transition metal dichalcogenides (TMDs) are the most widely studied 2D semiconductor materials. BP is a typical p-type 2D layered semiconductor with direct bandgap,^{1,2} high mobility for both electrons and holes,^{3–5} and widely tunable bandgap.^{2,6} Numerous works have studied the photodetectors based on BP and BP heterostructures with fast response,^{7,8} with polarization-sensitive photodetection,^{9,10} and integrated with a waveguide.^{11,12} The photovoltaic photoresponse of BP p–n junctions was fabricated by local electrostatic gating,¹³ Al doping,¹⁴ and vertical p–n junction induced by an ionic gel gated.¹⁰ The layer number dependent bandgap of BP shown in the previous literature indicates that the bandgap is very close to the bulk form of 0.3 eV as the thickness of BP flake is larger than 6.5 nm. The photodetectors based on BP exhibit high sensitive mid-wave infrared (MWIR) response, with a photoresponsivity of 82 A/W at 3.39 μm.¹⁵ Photodetectors based on BP

with fast photoresponse allow the black-body radiation response.^{9,16} However, BP is unstable in the ambient air,¹⁷ which hindered the wide application of BP photodetectors. TMDs have also been heavily investigated in recent years due to strong light–matter interaction¹⁸ bandgap covering a wide range from 0 to 2.5 eV,¹⁹ tunable electronic transport properties, and good stability in the air.^{20–22} Narrow bandgap TMDs, such as PtSe₂,^{23,24} PtTe₂,^{25–27} PdSe₂,²⁸ and PdTe₂,²⁹ are promising for uncooled MWIR and LWIR photodetection.³⁰ PdSe₂ is one of the most promising materials in uncooled MWIR and LWIR photodetection due to the properties of a narrow bandgap of 0.03 eV in the bulk form,²⁸ high mobility (~216 cm²/Vs), and tunable ambipolar characteristics,²³ in-plane anisotropic.^{25,31} Broadband photodetection based on PdSe₂ and its heterostructure from visible to near-infrared were demonstrated.^{32,33} The polarization-sensitive photodetection based on PdSe₂ was demonstrated with a high dichroic ratio of 2.2.²⁵ Based on PdSe₂, polarization-sensitive

and broadband photodetection were demonstrated.³⁴ The performance of the PdSe₂ detector can be enhanced by ozone treatment.³⁵ PdSe₂ has been proposed in several electronic applications, for instance, in ambipolar transistors³⁶ and field emission devices.³⁷ Moreover, high-performance LWIR detection based on PdSe₂ and its heterostructure were demonstrated with 42.1 A/W at 10.6 μm .²⁰ However, room temperature operation 2D material MWIR and LWIR photodetectors are suffering the low photoresponsivity, slow speed, and high current noise power intensity. To overcome these issues, we designed the BP/PdSe₂ heterodiode set on a metal electrode. To date, the uncooled MWIR and LWIR photodetection based on BP/PdSe₂ van der Waals (vdW) p-n junction remains elusive. The large bottom electrode is used as a mirror electrode to enhance light absorption. Furthermore, the bottom electrode can short the carrier lateral transport distance and realize a high efficiency in photocarrier collection and fast photoresponse.

To study the photoresponse of the BP/PdSe₂ van der Waals heterodiode, the high-quality BP/PdSe₂ device was fabricated. For the details, see the [supplementary material](#). The high-quality PdSe₂ single-crystal was grown using the self-flux method. The quality of the crystal was checked by energy-dispersive x-ray spectroscopy (EDX) and XRD spectral, as shown in Figs. S1(a) and S1(b), respectively. PdSe₂ field-effect transistors (FET) were fabricated using the standard electron beam lithography (EBL) followed by electron beam evaporation electrodes, as shown in Fig. S2(a). The thickness of the PdSe₂ FET is ~ 60 nm, which was checked by atomic force microscopy (AFM), as shown in Fig. S2(b). The transfer curve of the device at a bias of 0.1 V is presented in Fig. S2(c). A bipolar transport characteristic is observed.³⁸ The electron mobility of the PdSe₂ of ~ 37.8 cm²/V s is

obtained. The bipolar transport characteristic is also observed in another FET device with different thicknesses of ~ 32 nm, as shown in Figs. S2(d)–S2(f). At first, we designed a vdW heterodiode of the BP/PdSe₂ photodetector, which was placed on a predisposed gold electrode to enhance the light absorption, as shown in Fig. 1(a). The left panel of Fig. 1(b) shows the band profile of the PdSe₂ and BP before contact. The work function of BP (~ 4.8 eV)³⁹ is larger than that of PdSe₂ (~ 4.7 eV).⁴⁰ After contact, electrons were transferred from PdSe₂ to BP. The bandgap of BP (0.3 eV)¹ and PdSe₂ (0.03 eV)²⁸ is absorbers of MWIR and LWIR, respectively, as shown in the right panel of Fig. 1(b). Raman spectra of PdSe₂ and BP of a device are shown in the upper panel of Fig. 1(c), which is well consistent with the previous works.^{5,21} Figure 1(d) shows the AFM image of a typical PdSe₂/BP heterodiode device. The thickness of PdSe₂ is ~ 54.8 nm, and BP is ~ 20.6 nm as shown in Figs. S3(a) and S3(b), respectively.

Next, we investigate the photoresponse of the BP/PdSe₂ heterodiode at the visible range. Figure 2(a) presents the I - V curves of different incident light powers (4.0 nW–3.18 μW) and at dark. As the light power increased, the current increased notably. To evaluate the performance of the detector, we measured the time-resolved photoresponse at 1 V bias by varying the illumination powers of the 637-nm laser, as shown in Fig. 2(b). The extracted photocurrent vs light power is shown in Fig. 2(c). A sub-linear light power dependence behavior $I_p \propto P^\alpha$ is observed with $\alpha = 0.98$. Then, we calculate the photoresponsivity (R) and external quantum efficiency (EQE), which are defined as the ratio of photocurrent I_p to the incident light power and the number of photoexcited charge carriers forming photocurrent to the number of incident photons, respectively. The $R = I_p/P$ and EQE can be

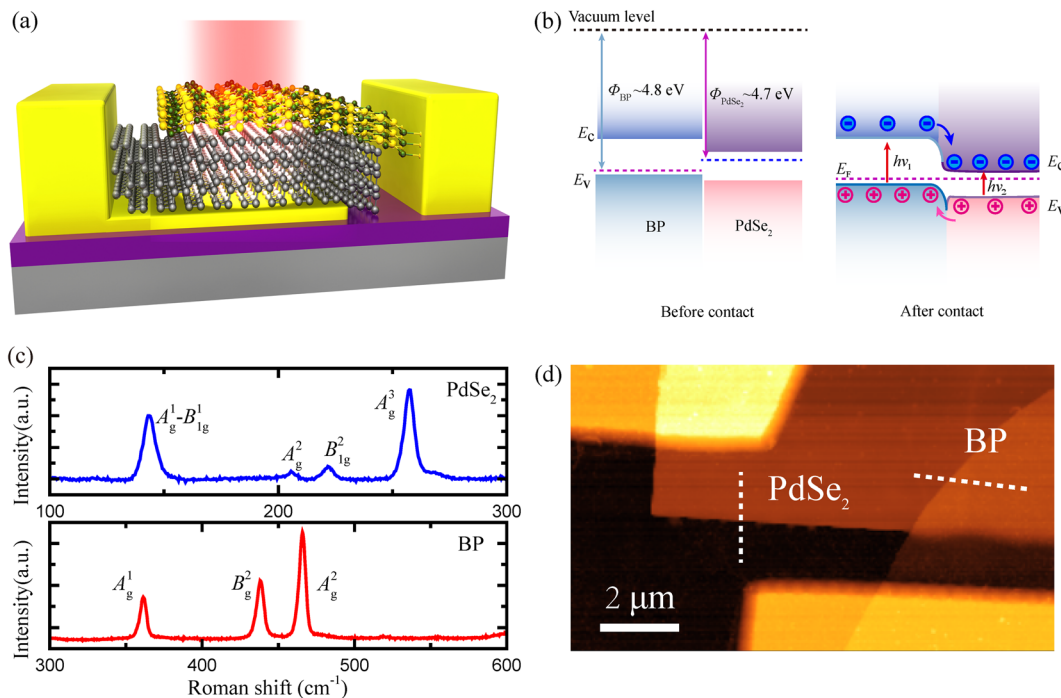


FIG. 1. PdSe₂/BP heterodiode photodetector structure. (a) Schematic image of the PdSe₂/BP heterodiode photodetector. (b) Band alignment of the PdSe₂/BP heterostructure. (c) Top panel and bottom panel shows the Raman spectrum of PdSe₂ flake and BP flake, respectively. (d) Atomic force microscopic image of the PdSe₂/BP heterostructure.

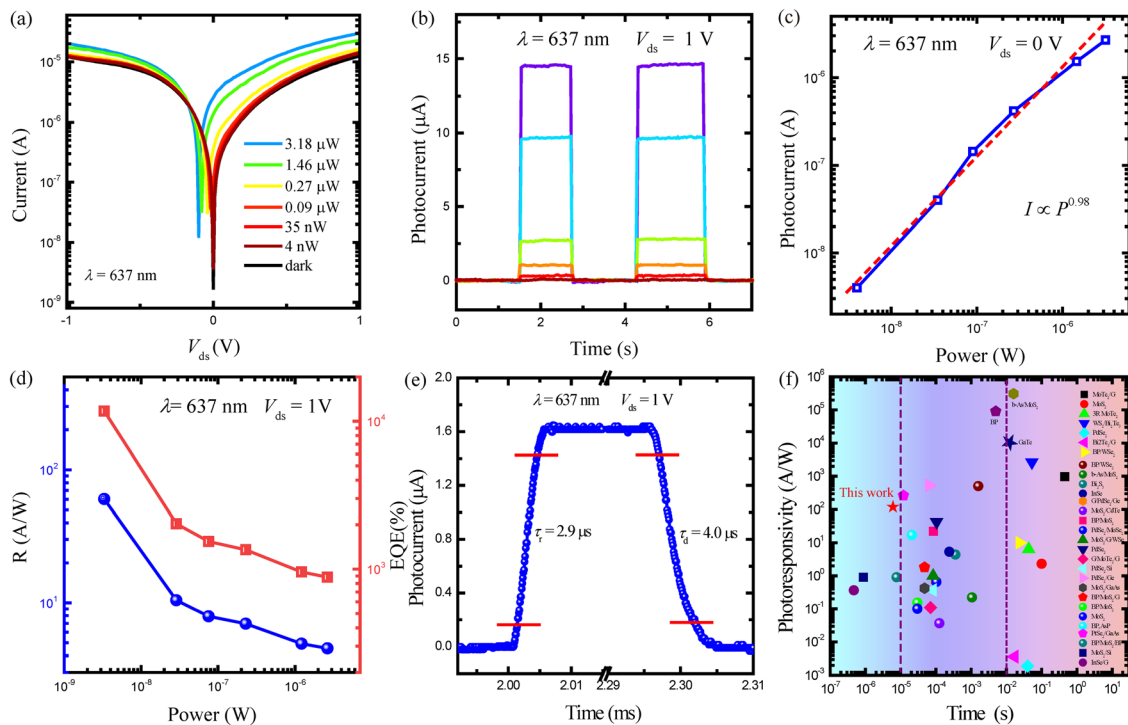


FIG. 2. Photoresponse of the PdSe₂/BP heterodiode device in the visible range. (a) Output curves of the PdSe₂/BP heterodiode device in the dark and under various incident light powers of a 637-nm laser. The incident light power ranges from 4 nW to 3.18 μW. (b) The temporal photoresponse under various incidence light powers of the 637-nm laser at a bias of 1 V. (c) Incident light power dependence photocurrent of a PdSe₂/BP heterodiode devices at a bias of $V_{ds} = 0$ V. (d) R (left axis) and EQE (right axis) of a typical PdSe₂/BP heterodiode device vs incident light power at a bias of 1 V. (e) The rise time of $\tau_r = 2.9$ μs and decay time of $\tau_d = 4.0$ μs for a typical PdSe₂/BP heterodiode at a bias of $V_{ds} = 1$ mV under the 637-nm laser. (f) R and response time summary of 2D material photodetectors.

expressed as $EQE = Rhc/e\lambda$, where h is Planck's constant, c is the speed of light, e is the elementary charge, and λ is the wavelength of the incident light. Figure 2(d) plots the light power-dependent R and EQE of the device at 1 V bias. The R of 60.3 A/W and EQE of 11 742.1% are obtained at 3.3 nW. As the light power increasing, the R decreased to 4.5 A/W and EQE decreased to 881.4% as the light power increased to 2.65 μW. The speed of the photoresponse is one of the most important figure-of-merit for photodetectors. The response speed of the device is usually evaluated by rising time (τ_r) and decay time (τ_d), which are defined as from 10% to 90% of the stable photocurrent as the laser was switched on and from 90% to 10% of the stable photocurrent as the laser was switched off, respectively. The rise time $\tau_r = 2.9$ μs and the decay time $\tau_d = 4.0$ μs were obtained under a 637-nm laser in Fig. 2(e). The speed of this device is much faster than those of the other 2D material photodetectors, as shown in Fig. 2(f). The performance of the 2D-base photodetectors is summarized in Table S1 in the support information. The time-resolved photoresponse under various incident light powers of 405-nm laser at a bias of 1 V is presented in Fig. S4(a). The extracted R and EQE are plotted in Fig. S4(b). When the device is under an incident light power of 50 nW, the R of 3.0 A/W and the EQE of 918.5% were realized. The temporal photoresponse of the 405-nm laser at a bias of 1 mV is presented in Fig. S4(c). The frequency of switching on/off the light is 1 kHz. After a few tens of cycles of the switch on/off the light, the photoresponse was very fast and stable. The response time of the PdSe₂/BP heterodiode is presented in Fig. S5(d).

The rise time of $\tau_r = 3.0$ μs and the decay time of $\tau_d = 4.8$ μs were demonstrated at a bias of 1 mV under a 405-nm laser. The fast response speed could be attributed to the vertical device structure with a very short transport distance and large mirror electrode realizing good Ohmic contact.

Next, we investigate the performance of this device in the near-infrared region from 830 to 1310 nm. The temporal photoresponse of 940 nm at a bias of 1 V under varying incident light power is shown in Fig. 3(a). The photocurrent of 21.7 μA is obtained as the incident light power is 1.16 μW. Figure 3(b) is the power dependence of R and EQE at a 1 V bias of the 940 nm laser. The photoresponsivity of 116.1 A/W and the EQE of 15 302.1% was demonstrated at incident light power of 0.6 nW. As the incident light powers increase, a decreasing tendency of the R and EQE is observed. The R drop from 116.1 to 3.44 A/W as the light power increases from 0.6 nW to 1.16 μW, corresponding EQE decrease from 15 302.1% to 453.8%. The I - V curves with varying the incident light power of a PdSe₂/BP heterodiode are plotted in Fig. S5(a). The temporal photoresponse with varying the incident light (830 nm laser) power is shown in Fig. S5(b). The photocurrent of 12.1 μA was realized under 8.48 μW illumination. The sharply increased photocurrent as the laser switch on indicates the fast photoresponse of the heterodiode. Then, we measured the response time of the device under the illumination of an 830-nm laser. As shown in Figs. S5(c) and S5(d), the rise time is $\tau_r = 22.4$ μs and the decay time is $\tau_d = 12.2$ μs at a bias of 1 V, respectively. The performance of the

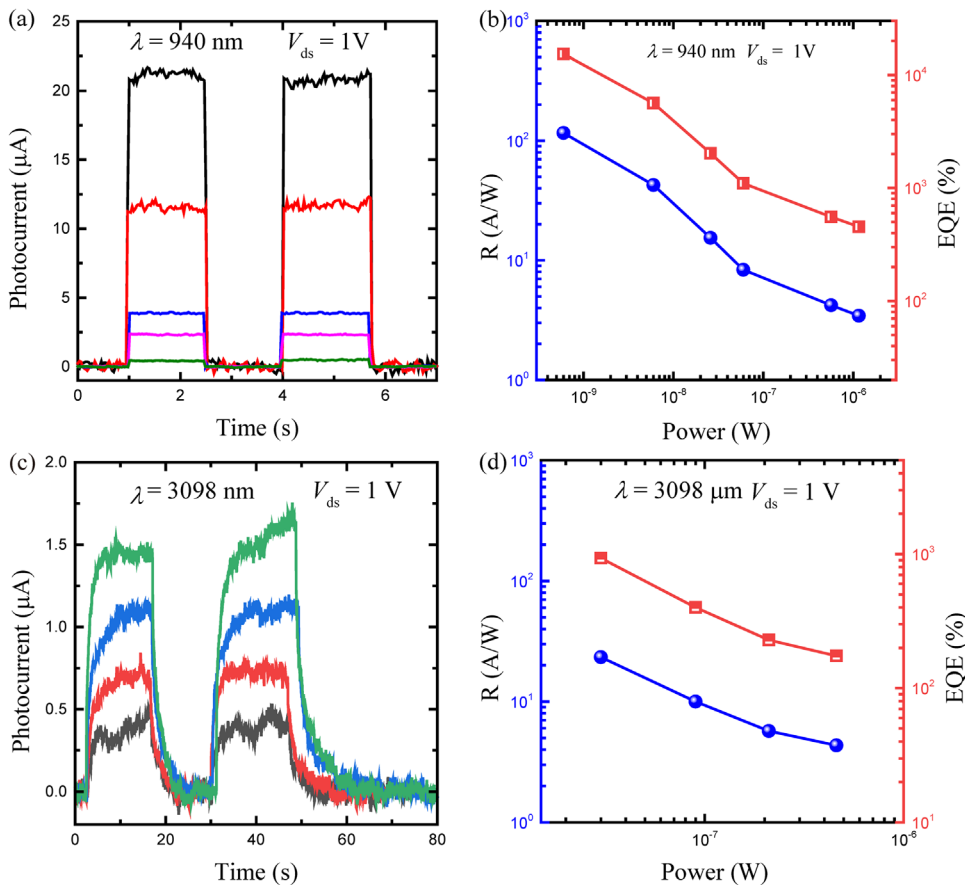


FIG. 3. Photoresponse of the PdSe₂/BP heterodiode device in SWIR and MWIR ranges. (a) and (c) The temporal photoresponse under various incidence light powers of the 940-nm laser and the 3098-nm laser at a bias of $V_{ds} = 1$ V, respectively. (b) and (d) Extracted R (left axis) and EQE (right axis) of a typical PdSe₂/BP heterodiode device vs incident light power 940-nm laser and 3098-nm laser at a bias of $V_{ds} = 1$ V.

device in the SWIR range of 1310 nm was investigated. As presented in Fig. S6(a), the I - V curves at different incident powers and dark were measured. As the light power increases, the photocurrent increased considerably. To evaluate the performance of the detector in this range, the time-resolved photoresponse at a bias of 1 V with varying incident light powers is presented in Fig. S6(b). A photocurrent of 18.8 μ A is realized under 1.3 μ W illumination at a bias of 1 V. The incident light power dependence R and EQE are presented in Fig. S6(c). The R of 71.4 A/W and the EQE of 6760.4% were demonstrated when the light power is 1.4 nW at a bias of 1 V. As the incident light power increases, a decreasing tendency of the R and EQE is exhibited. The R decreased to 3.2 A/W, and the corresponding EQE decreased to 306.7% as the light power increased to 1.3 μ W.

Next, we investigate the photoresponse of the device in the MWIR range from 2611 to 4117 nm. Figure 3(c) presents the time-resolved photoresponse of a 3098 nm laser with varying illumination powers at a bias of 1 V. The photocurrent of 1.5 μ A is obtained as the device was exposed to the illumination of 0.46 μ W. The incident light power dependence R and EQE at a bias of 1 V are plotted in Fig. 3(d). The R and EQE decreased as the illumination power increased. As the incident power decreased to 30 nW, the R of 23.3 A/W and the EQE of 933.8% are realized. The temporal photoresponse with various incident light powers of 2611 and 3662 nm is shown in Fig. S7(a) and S7(b), respectively. Figure S7(c) presents the time-resolved photoresponse under

various incident powers of the 3662-nm laser at a bias of 10 mV. The extracted R and EQE vs light power of 2611 and 3662 nm are presented in Figs. S7(d) and S7(e), respectively. The R up to 30.1 A/W and the corresponding EQE of 1424.7% were demonstrated under 40 nW illumination. For the 3662 nm laser, the R of 8.9 A/W and the EQE of 304.1% are obtained under 90 nW illumination at a bias of 1 V. The speed of the device in the MWIR range was measured, as shown in Fig. S7(f). The rise time $\tau_r = 1.3$ ms and decay time $\tau_d = 1.5$ ms were demonstrated at a bias of 10 mV. For the temporal photoresponse in the MWIR range, the response includes two parts, as shown in Fig. S8. The fast response of the initial rising process with a speed of 0.507 μ A/s and the slow response process with a speed of 0.022 μ A/s could be attributed to the photothermal effect. The mechanism of the photocurrent generation for this range may originate from the photo-bolometer effect.²² The response time is much lower than the thermal time constant of 15 ms. Then, the performance of the PdSe₂/BP heterodiode at the LWIR 10.6 μ m was characterized. The temporal photoresponse at a 1 V bias with varying incident illumination power is shown in Fig. S9(a). The extracted R and EQE vs illumination powers are presented in Fig. S9(b). The R of 2.2 A/W and the EQE of 26.3% were realized at a bias of 1 V under the illumination of 80 nW. The temporal photoresponses at biases of 1 mV and 0 V varying the wavelengths of incident laser from 1310 to 4117 nm are shown in Figs. S10 and S11, respectively. The extracted R and EQE as a function of wavelength at a bias of 1 mV are

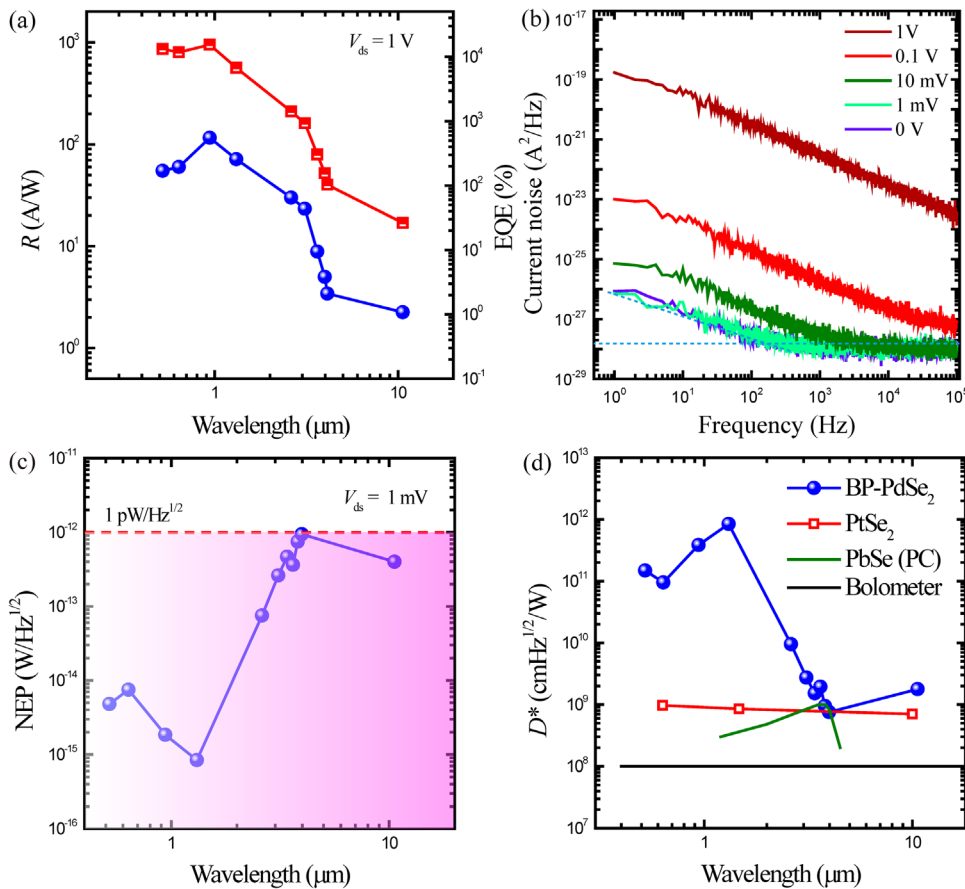


FIG. 4. Wavelength dependence photo-response of PdSe₂/BP heterodiode device. (a) R (left) and EQE (right) of a typical PdSe₂/BP heterodiode device as a function of wavelength at a bias of 1 V. (b) The current noise density spectra at different biases. (c) Wavelength dependence of the noise equivalent power (NEP) at a bias of 1 mV. (d) D^* as a function of incident light power. Compared D^* with commercially available infrared detectors and the state-of-the-art 2D LWIR photodetectors.

plotted in Fig. S12. The R of 1.84 A/W and the corresponding EQE of 73.6% were demonstrated under the illumination of 38.0 nW. The wavelength dependence R and EQE at 1 V bias are presented in Fig. 4(a). From visible 520 to 940 nm, the R increased from 55.1 to 116.0 A/W, the corresponding EQE increased from 13 115.4% to 15 302.1%. Then, as the wavelength increases, a decreased tendency of R and EQE was exhibited. The R decreased from 30.1 to 3.4 A/W from 2611 to 4117 nm and then decreased to 2.2 A/W as the wavelength increased to LWIR 10.6 μm . To evaluate the noise equivalence power (NEP), which is used to assess the detection limit of a detector, we measured the current noise power spectra at various bias voltages, as shown in Fig. 4(b); for the details, see the supplementary material. Figure 4(c) presents the NEP as a function of wavelength at a bias of 1 mV. The dashed red line is placed on $1\text{ pW}/\text{Hz}^{1/2}$. From visible to the LWIR, the NEP is lower than the $1\text{ pW}/\text{Hz}^{1/2}$ line. In the telecommunication range of 1310 nm, the device exhibits a very low NEP of $8.4 \times 10^{-16}\text{ W}/\text{Hz}^{1/2}$. Then, we calculated the specific detectivity, which is one of the most important figures of merit of a photodetector, by $D^* = (A\Delta f)^{1/2}/\text{NEP}$, where A is the active area of the device and Δf is the measuring bandwidth. For the PdSe₂/BP heterostructure device, D^* of $8.45 \times 10^{11}\text{ cm}^2\text{Hz}^{1/2}/\text{W}$ is realized at 1310 nm, of $1.1 \times 10^{10}\text{ cm}^2\text{Hz}^{1/2}/\text{W}$ in MWIR range 2611 nm, and $2.05 \times 10^9\text{ cm}^2\text{Hz}^{1/2}/\text{W}$ was obtained at LWIR 10.6 μm in ambient air, as shown in Fig. 4(d). In the MWIR range, the D^* ranges from 1.09×10^{10} to $1.21 \times 10^9\text{ cm}^2\text{Hz}^{1/2}/\text{W}$, which is slightly higher than that of commercially available PbSe MWIR

photodetector, bolometer D^* of $10^8\text{ cm}^2\text{Hz}^{1/2}/\text{W}$,⁴¹ and 2D LWIR PtSe₂ $7 \times 10^8\text{ cm}^2\text{Hz}^{1/2}/\text{W}$.³⁰

In summary, we demonstrated an ultrabroad band photoresponse from the visible to LWIR range (520 nm–10.6 μm) based on a PdSe₂/BP heterodiode. The high photoresponsivity of 116.0 A/W, the specific detectivity of $8.45 \times 10^{11}\text{ cm}^2\text{Hz}^{1/2}/\text{W}$, and a low NEP of $8.4 \times 10^{-16}\text{ W}/\text{Hz}^{1/2}$ were realized at the 1310-nm laser. The photo-response speed of the PdSe₂/BP heterodiode is very fast with $\tau_r = 2.9$ and $\tau_d = 4.0\text{ }\mu\text{s}$. The device exhibits a room temperature response. The photoresponsivity up to 2.2 A/W and D^* of $2.05 \times 10^9\text{ cm}^2\text{Hz}^{1/2}/\text{W}$ were obtained in the LWIR 10.6 μm . Our proposed device architecture provides a strategy to design high-performance photodetectors with promising applications in broadband and fast-speed response photodetection.

See the supplementary material for the XRD, EDX, and AFM characterization of the quality of PdSe₂ single-crystal, the transport curves of PdSe₂ FETs, and additional data for the performance of photodetector at 405 and 830-nm laser and the performance from the short-wave infrared 1310 nm to long-wave infrared 10.6 μm spectra range.

This work was supported by the National Natural Science Foundation of China (Grant Nos. 61975224 and 12074002),

University Synergy Innovation Program of Anhui Province (Grant No. GXXT-2020-050), Fund of Anhui Provincial Natural Science Foundation (Grant No. 2008085MF206), the Recruitment Program for Leading Talent Team of Anhui Province 2020, State Key Laboratory of Luminescence and Applications (Grant No. SKLA-2021-03), the Open Fund of Infrared and Low-Temperature Plasma Key Laboratory of Anhui Province (Grant No. IRKL2022KF03), and the Jiaxing Science and Technology Project Grant (No. 2021AY10057).

AUTHOR DECLARATIONS

Conflict of Interest

The authors have no conflicts to disclose.

Author Contributions

Qingsong Dong: Investigation (lead); writing – original draft (equal). **Fang Wang:** Investigation (lead); writing – original draft (equal). **Xin Hu:** Investigation (supporting). **Yuan Lu:** Investigation (supporting). **Dongxu Zhao:** Investigation (supporting). **Min Zhang:** Funding acquisition (equal); investigation (supporting). **Tao Han:** Investigation (supporting). **Xingyuan Hou:** Investigation (supporting). **Shaoliang Wang:** Investigation (supporting). **Mingsheng Long:** Funding acquisition (lead); investigation (lead); supervision (lead); writing – original draft (lead); writing – review & editing (lead). **Lei Shan:** Funding acquisition (equal).

DATA AVAILABILITY

The data that support the findings of this study are available from the corresponding authors upon reasonable request.

REFERENCES

- X. Wang, A. M. Jones, K. L. Seyler, V. Tran, Y. Jia, H. Zhao, H. Wang, L. Yang, X. Xu, and F. Xia, *Nat. Nanotechnol.* **10**, 517–521 (2015).
- V. Tran, R. Soklaski, Y. Liang, and L. Yang, *Phys. Rev. B* **89**, 235319 (2014).
- L. Li, G. J. Ye, V. Tran, R. Fei, G. Chen, H. Wang, J. Wang, K. Watanabe, T. Taniguchi, L. Yang, X. H. Chen, and Y. Zhang, *Nat. Nanotechnol.* **10**, 608–614 (2015).
- J. Qiao, X. Kong, Z.-X. Hu, F. Yang, and W. Ji, *Nat. Commun.* **5**, 4475 (2014).
- H. Liu, A. T. Neal, Z. Zhu, Z. Luo, X. Xu, D. Tománek, and P. D. Ye, *ACS Nano* **8**, 4033–4041 (2014).
- X. Chen, X. Lu, B. Deng, O. Sinai, Y. Shao, C. Li, S. Yuan, V. Tran, K. Watanabe, T. Taniguchi, D. Naveh, L. Yang, and F. Xia, *Nat. Commun.* **8**, 1672 (2017).
- H. Liu, M. Köpf, A. N. Abbas, X. Wang, Q. Guo, Y. Jia, F. Xia, R. Wehrich, F. Bachhuber, F. Pielhofer, H. Wang, R. Dhall, S. B. Cronin, M. Ge, X. Fang, T. Nilges, and C. Zhou, *Adv. Mater.* **27**, 4423–4429 (2015).
- M. Buscema, D. J. Groenendijk, S. I. Blanter, G. A. Steele, H. S. J. van der Zant, and A. Castellanos-Gomez, *Nano Lett.* **14**, 3347–3352 (2014).
- J. Bullock, M. Amani, J. Cho, Y.-Z. Chen, G. H. Ahn, V. Adinolfi, V. R. Shrestha, Y. Gao, K. B. Crozier, Y.-L. Chueh, and A. Javey, *Nat. Photonics* **12**, 601–607 (2018).
- H. Yuan, X. Liu, F. Afshinmanesh, W. Li, G. Xu, J. Sun, B. Lian, A. G. Curto, G. Ye, Y. Hikita, Z. Shen, S.-C. Zhang, X. Chen, M. Brongersma, H. Y. Hwang, and Y. Cui, *Nat. Nanotechnol.* **10**, 707–713 (2015).
- C. Lin, R. Grassi, T. Low, and A. S. Helmy, *Nano Lett.* **16**, 1683–1689 (2016).
- N. Youngblood, C. Chen, S. J. Koester, and M. Li, *Nat. Photonics* **9**, 247–252 (2015).
- M. Buscema, D. J. Groenendijk, G. A. Steele, H. S. J. van der Zant, and A. Castellanos-Gomez, *Nat. Commun.* **5**, 4651 (2014).
- Y. Liu, Y. Cai, G. Zhang, Y.-W. Zhang, and K.-W. Ang, *Adv. Funct. Mater.* **27**, 1604638 (2017).
- Q. Guo, A. Pospischil, M. Bhuiyan, H. Jiang, H. Tian, D. Farmer, B. Deng, C. Li, S.-J. Han, H. Wang, Q. Xia, T.-P. Ma, T. Mueller, and F. Xia, *Nano Lett.* **16**, 4648–4655 (2016).
- M. Amani, E. Regan, J. Bullock, G. Ho Ahn, and A. Javey, *ACS Nano* **11**, 11724–11731 (2017).
- J. O. Island, G. A. Steele, H. S. J. van der Zant, and A. Castellanos-Gomez, *2D Mater.* **2**, 011002 (2015).
- L. Britnell, R. M. Ribeiro, A. Eckmann, R. Jalil, B. D. Belle, A. Mishchenko, Y. J. Kim, R. V. Gorbachev, T. Georgiou, S. V. Morozov, A. N. Grigorenko, A. K. Geim, C. Casiraghi, A. H. Castro Neto, and K. S. Novoselov, *Science* **340**, 1311–1314 (2013).
- M. Long, P. Wang, H. Fang, and W. Hu, *Adv. Funct. Mater.* **29**, 1803807 (2019).
- M. Long, Y. Wang, P. Wang, X. Zhou, H. Xia, C. Luo, S. Huang, G. Zhang, H. Yan, Z. Fan, X. Wu, X. Chen, W. Lu, and W. Hu, *ACS Nano* **13**, 2511–2519 (2019).
- A. D. Oyedele, S. Yang, L. Liang, A. A. Puretzy, K. Wang, J. Zhang, P. Yu, P. R. Pudasaini, A. W. Ghosh, Z. Liu, C. M. Rouleau, B. G. Sumpter, M. F. Chisholm, W. Zhou, P. D. Rack, D. B. Geohegan, and K. Xiao, *J. Am. Chem. Soc.* **139**, 14090–14097 (2017).
- Y. Wang, P. Wu, Z. Wang, M. Luo, F. Zhong, X. Ge, K. Zhang, M. Peng, Y. Ye, Q. Li, H. Ge, J. Ye, T. He, Y. Chen, T. Xu, C. Yu, Y. Wang, Z. Hu, X. Zhou, C. Shan, M. Long, P. Wang, P. Zhou, and W. Hu, *Adv. Mater.* **32**, 2005037 (2020).
- W. L. Chow, P. Yu, F. Liu, J. Hong, X. Wang, Q. Zeng, C.-H. Hsu, C. Zhu, J. Zhou, X. Wang, J. Xia, J. Yan, Y. Chen, D. Wu, T. Yu, Z. Shen, H. Lin, C. Jin, B. K. Tay, and Z. Liu, *Adv. Mater.* **29**, 1602969 (2017).
- Y. Zhao, J. Qiao, Z. Yu, P. Yu, K. Xu, S. P. Lau, W. Zhou, Z. Liu, X. Wang, W. Ji, and Y. Chai, *Adv. Mater.* **29**, 1604230 (2017).
- L. Pi, C. Hu, W. Shen, L. Li, P. Luo, X. Hu, P. Chen, D. Li, Z. Li, X. Zhou, and T. Zhai, *Adv. Funct. Mater.* **31**, 2006774 (2021).
- D. A. Nguyen, D. Y. Park, J. Lee, N. T. Duong, C. Park, D. H. Nguyen, T. S. Le, D. Suh, H. Yang, and M. S. Jeong, *Nano Energy* **86**, 106049 (2021).
- X.-W. Tong, J.-J. Wang, J.-X. Li, X.-F. Hu, D. Wu, and L.-B. Luo, *Sens. Actuators, A* **322**, 112625 (2021).
- J. Sun, H. Shi, T. Siegrist, and D. J. Singh, *Appl. Phys. Lett.* **107**, 153902 (2015).
- C. Guo, Y. Hu, G. Chen, D. Wei, L. Zhang, Z. Chen, W. Guo, H. Xu, C.-N. Kuo, C. S. Lue, X. Bo, X. Wan, L. Wang, A. Politano, X. Chen, and W. Lu, *Sci. Adv.* **6**, b6500 (2020).
- X. Yu, P. Yu, D. Wu, B. Singh, Q. Zeng, H. Lin, W. Zhou, J. Lin, K. Suenaga, Z. Liu, and Q. J. Wang, *Nat. Commun.* **9**, 1545 (2018).
- A. M. Afzal, M. Z. Iqbal, G. Dastgeer, A. U. Ahmad, and B. Park, *Adv. Sci.* **8**, 2003713 (2021).
- L. Pi, P. Wang, S.-J. Liang, P. Luo, H. Wang, D. Li, Z. Li, P. Chen, X. Zhou, F. Miao, and T. Zhai, *Nat. Electron.* **5**, 248–254 (2022).
- F. Wang, P. Luo, Y. Zhang, Y. Huang, Q. Zhang, Y. Li, and T. Zhai, *Sci. China Mater.* **63**, 1537–1547 (2020).
- D. Wu, J. Guo, J. Du, C. Xia, L. Zeng, Y. Tian, Z. Shi, Y. Tian, X. J. Li, Y. H. Tsang, and J. Jie, *ACS Nano* **13**, 9907–9917 (2019).
- Q. Liang, Q. Zhang, J. Gou, T. Song, Arramel, H. Chen, M. Yang, S. X. Lim, Q. Wang, R. Zhu, N. Yakovlev, S. C. Tan, W. Zhang, K. S. Novoselov, and A. T. S. Wee, *ACS Nano* **14**, 5668–5677 (2020).
- A. D. Bartolomeo, F. Urban, A. Pelella, A. Grillo, M. Passacantando, X. Liu, and F. Giubileo, *Nanotechnology* **31**, 375204 (2020).
- A. D. Bartolomeo, A. Pelella, F. Urban, A. Grillo, L. Iemmo, M. Passacantando, X. Liu, and F. Giubileo, *Adv. Electron. Mater.* **6**, 2000094 (2020).
- A. Pelella, X. Liu, and A. D. Bartolomeo, *Adv. Funct. Mater.* **29**, 1902483 (2019).
- X. Liu, D. Qu, H.-M. Li, I. Moon, F. Ahmed, C. Kim, M. Lee, Y. Choi, J. H. Cho, J. C. Hone, and W. J. Yoo, *ACS Nano* **11**, 9143–9150 (2017).
- L.-H. Zeng, D. Wu, S.-H. Lin, C. Xie, H.-Y. Yuan, W. Lu, S. P. Lau, Y. Chai, L.-B. Luo, Z.-J. Li, and Y. H. Tsang, *Adv. Funct. Mater.* **29**, 1806878 (2019).
- M. Long, A. Gao, P. Wang, H. Xia, C. Ott, C. Pan, Y. Fu, E. Liu, X. Chen, W. Lu, T. Nilges, J. Xu, X. Wang, W. Hu, and F. Miao, *Sci. Adv.* **3**, e1700589 (2017).